ARTICLES

Structural and Electronic Properties of Sol−Gel Titanium Oxides Studied by X-ray Absorption Spectroscopy

Vittorio Luca,* Samitha Djajanti, and Russell F. Howe

School of Chemistry, University of New South Wales, Sydney 2052, Australia

Received: March 26, 1998; In Final Form: October 10, 1998

X-ray absorption spectroscopy (XAS) has been used to study the local Ti environment in titania xerogel samples containing nanoparticles of different sizes. The xerogels were prepared by hydrolysis of titanium isopropoxide followed by peptization with HNO_3 and size control was achieved through calcination in air at different temperatures. An amorphous precipitate obtained by hydrolysis of titanium isopropoxide prior to peptization with HNO_3 has also been studied. The X-ray absorption near edge structure (XANES) of the precipitate possesses a characteristic preedge that is dominated by a transition designated as A2 at 4970.7 eV, and assigned to five coordinate Ti. This A2 component is detected in all of the studied xerogels. Its intensity decreases as the surface-to-volume ratio of the titania particles decreases, suggesting that it is associated with surface layers of the anatase particles. Other changes observed in the XANES of the xerogels as a function of particle size include broadening of $1s \rightarrow np$ transitions in the postedge region. EXAFS shows that the smallest particles contain Ti in distorted coordination with contracted Ti−O bonds and probably reduced coordination number.

Introduction

Titania produced by the hydrolysis and subsequent peptization of titanium alkoxides in the form of colloids, xerogel powders, and thin films has become an important technological material in the fields of photocatalysis, photovoltaics, and electrooptics. In photocatalysis, it is the anatase form of titania that appears to be the most active.[1] It is also this form of titania that has been intensively studied in the past 10 years since the discovery by Grätzel and co-workers[2] that films made from anatase sols when functionalized with ruthenium complexes could be used to make efficient solar cell devices. The anatase sol used in these applications is often produced through a sol−gel route involving the hydrolysis of titanium isopropoxide followed by peptization using a strong acid such as HNO_3.[3]

While there have been several recent studies devoted to gaining an understanding of the microstructure of sol−gel anatase films and powders using electron microscopic techniques,[4,5] there have been few studies of the finer structural details of the nanoparticles. In this regard it is important to know the coordination number, degree of TiO_6 condensation, the atomic structure of the gel network in each particle as a function of depth from the surface, defect type and population, etc. A detailed picture of the surface and bulk structural properties of these nanocrystalline materials is extremely important since these can be pivotal in controlling physicochemical and electronic properties. In connection with the photocatalytic properties of titania sols, it is becoming increasingly recognized that surface states play an important role in electron trapping[6] and that a poorly crystalline surface would have considerably more trapping sites. However, there is little or no information on the surface structure of nanocrystalline titania particles that make up such gels. The coordination number of surface titanium is especially important as the degree of coordinative saturation of the titanium can influence surface adsorption and surface acidity.

X-ray absorption spectroscopy (XAS) is a technique that is atom specific and capable of probing the short to medium range structure around an imbedded or absorbing atom. Whereas in X-ray diffraction a minimum coherent scattering domain is necessary, this is not the case in X-ray absorption, which can therefore be applied to the study of liquids and X-ray amorphous materials. In this respect X-ray absorption is the complement of X-ray diffraction.

In this study we examine the XAS of anatase xerogel samples that contain nanocrystalline particles of different size and show that XAS can provide information on the local structure around the titanium atom as a function of particle size. This work also attempts to add to an understanding of the relationship between the structure of nanocrystalline anatase and associated electronic properties.

Experimental Section

An amorphous titania precipitate was synthesized by the dropwise addition of titanium isopropoxide (Aldrich) to milli-Q water to generate a white precipitate. The resulting suspension was stirred for 30 min and then filtered, thoroughly washed with milli-Q water, and dried at 30 °C. Colloidal titania sols

* Author for correspondence. Present address: Materials Division, Australian Nuclear Science and Technology Organization, PMB 1 Menai NSW 2234, Australia. FAX: 61-2-9543 7179. E-mail: vlu@ansto.gov.au.

10.1021/jp981644k CCC: $15.00
Published on Web 12/08/1998

were produced by the addition of HNO_3 to the suspension followed by peptization at 80 °C for about 24 h in an open beaker to facilitate the evaporation of the propanol generated through the hydrolysis of the alkoxide. This method is similar to that used in many studies of the photochemistry of sol−gel titania films and colloids.[3] The anatase sol was dried at 30 °C and then heated for 24 h in air at various temperatures.

X-ray absorption spectra were recorded in transmission mode on beam line 20B of the Australian National Beam line Facility (ANBF) at The Photon Factory, Tsukuba, Japan, using a Si-(111) monochromator and at the Stanford Synchrotron Radiation Laboratory (SSRL) on beam line 4-1 using a Si(220) monochromator. A measure of the relative resolution on these two stations for comparison with past and future results can be made from the peak-to-peak first-derivative line width of the first preedge feature in the titanium metal foil reference spectrum. These values were 1.42 eV for the ANBF data and 0.60 eV for SSRL data. The latter data were therefore more suitable for detailed consideration of the XANES while for EXAFS analysis we have analyzed data recorded with both Si(111) and Si(220) monochromators. Normalization of the spectra was performed using the program WINXAS,[7] which fits a zero-order spline to a specified region after the edge step. Analysis of the EXAFS was performed with the programs XFIT[8] and FEFFIT.[9] To avoid thickness effects, samples were diluted and thoroughly mixed with boron nitride. To fit the EXAFS, initial values of E0, the energy zero, and S_o^2, the amplitude reduction factor, were obtained by fitting the EXAFS of a crystalline anatase reference sample with the number of nearest-neighbor atoms (N), their distance (R), and the Debye−Waller factor (σ^2) fixed at their expected crystallographic values and allowing E0 and S_o^2 to float simultaneously. The obtained values of E0 and S_o^2 were then used as initial values for the modeling of the less crystalline samples.

XRD patterns were obtained using a Siemens D500 diffractometer using Cu Kα radiation. The step size used was 0.02° 2θ and the scan time was 1° 2θ/min.

Diffuse reflectance UV/vis spectra were recorded on a Cary 5 spectrometer using an integrating sphere accessory.

Transmission electron microscope images of the nanocrystalline particles were obtained of samples dispersed on a holy carbon coated copper grid using a JEOL 2000FX transmission electron microscope.

Results and Discussion

X-ray Diffraction/UV−Visible Spectra. Portions of the powder XRD patterns of selected samples relevant to the present study are shown in Figure 1, and the crystallite sizes determined from these data by integral breadth analysis[10] are given in Table 1. The XRD pattern of the precipitate dried at 30 °C (sample 1) shows only a very broad hump centered at 28° 2θ but no peaks, indicating that this material is X-ray amorphous. After aging in ambient air for several months (sample 2) the X-ray diffraction pattern changes to give a weak broad peak centered at the position of the anatase (101) reflection, which is superimposed on a broad background. This change with aging in ambient air is presumably due to increased condensation of Ti−OH groups to form Ti−O−Ti linkages with the loss of residual water. The materials derived from the dehydration of the titania sols (samples 3−5) show only the presence of anatase and no rutile, with the sample heated at 400 °C (sample 6) showing a minor rutile component. The average diameters of the particles comprising these dried sols increase from ~38 Å for sample 3, which was dried at 30 °C, to 110 Å for sample 6, which was heated in air at 400 °C. The commercial anatase that had also been heated at 400 °C (sample 7) exhibits far greater crystallinity compared with its sol−gel derived counterpart and has an average crystallite diameter of about 600 Å.

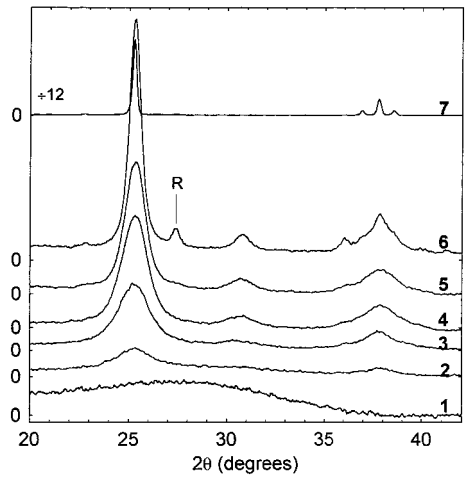

Figure 1. Powder XRD patterns of various titania samples described in Table 1. Sample numbers appear in bold down the right side of the figure.

TABLE 1: Particle Sizes Determined by the Integral Breadth Method and Direct Band Gap Energies for Anatase Samples Dried and Then Calcined at Various Temperatures

sample no.	temp (°C)	particle size (Å)[a]	E_g (eV)[b] ± 0.02
1. amorphous precipitate	30		3.66
2. amorphous precipitate (aged)	30	<20	3.66
3. anatase sol	30	38	3.42
4. anatase sol	200	51	3.41
5. anatase sol	300	65	3.37
6. anatase sol	400	110	3.33
7. anatase (Aldrich)	400	603	3.44

[a] From the integral breadth. [b] From plot of $(F(R) \times h\nu)^2$ versus $h\nu$.

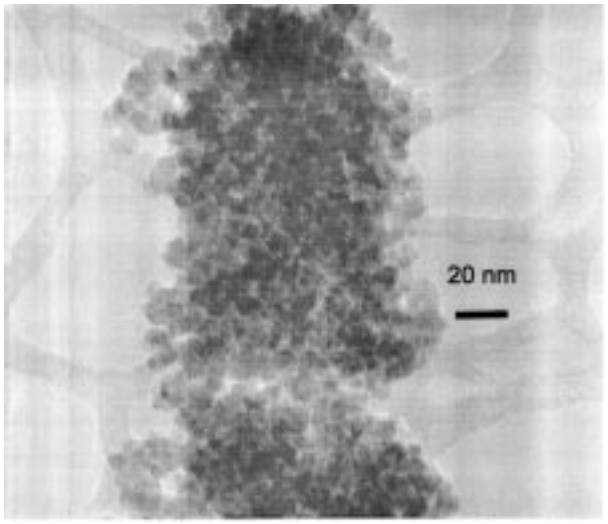

Figure 2. TEM image of dried xerogel calcined at 300 °C (sample 5).

A TEM image of the xerogel heated in air at 300 °C is shown in Figure 2 and demonstrates that the sample consists of loosely packed crystallites with rounded edges. The absence of faceting on the particles attests to the structural disorder. The average crystallite diameter measured from this image is about 60 ± 5 Å and agrees very well with the particle size measurement by

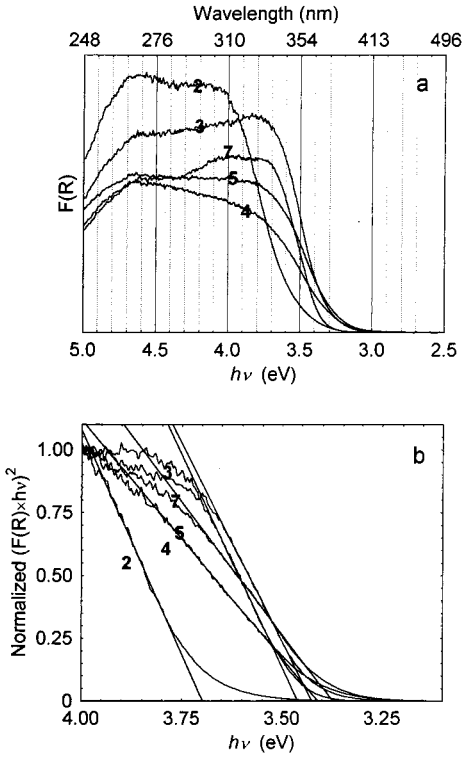

Figure 3. Diffuse reflectance UV−visible spectra of selected titania samples plotted as (a) $(F(R) \times h\nu)^2$ versus $h\nu$ and (b) normalized $(F(R) \times h\nu)^2$ versus $h\nu$ and showing the fit to the linear portion corresponding to the direct band gap transition.

XRD line broadening analysis. From comparisons of particle sizes obtained from XRD, TEM, and surface area measurements we estimate the average uncertainty in particle sizes measured by XRD to be about 20%.

UV−vis diffuse reflectance spectra of selected samples are shown in Figure 3a. The spectral envelopes are clearly the summations of a number of subspectra. Estimates of the optical band gap (E_g) can be obtained using the following equation for a semiconductor

$$a(\nu) = A(\hbar\nu - E_g)^{m/2} \quad (1)$$

where $\hbar = h/2\pi$, a is the absorption coefficient, and m is equal to 1 for a direct allowed transition. Since a is proportional to $F(R)$, the Kubelka−Munk function, then the energy intercept of a plot of $(F(R) \times h\nu)^2$ versus $h\nu$ (Figure 3b) gives E_g for a direct allowed transition when the linear region is extrapolated to zero ordinate. The linear region of these curves is limited to a range of 0.2−0.3 eV, and there is extensive tailing, which is particularly severe in the spectrum of sample 2. Similar results are obtained if $(F(R) \times h\nu)^{1/2}$ is plotted against $h\nu$, as is appropriate for an indirect semiconductor. For the present comparative exercise, however, we have opted to use the equation for a direct semiconductor in accordance with common practice.[11−13] The comparative band gap energies are summarized in Table 1, which shows a number of interesting features. For samples 1 and 2, E_g is 3.66 eV, which is about 0.2 eV higher than that obtained for the commercial anatase (sample 7), which gave a value of 3.44 eV. The E_g for the commercial sample agrees with the lowest energy direct transition in bulk anatase crystals.[14] The commercial anatase sample with the largest particle size of the samples investigated is blue shifted relative to the xerogels, which have E_g values ranging from 3.42 to 3.33 eV. The xerogels show only a weak dependence on particle size, being more blue shifted for smaller particles, as expected. The band gap values obtained for the xerogels are somewhat larger than those obtained for similar materials by Sanchez and Lopez[12] although their data also show little or no variation in E_g with calcination temperature.

Bahnemann[15] has recently measured blue shifts relative to bulk anatase of about 0.15 eV for TiO_2 particles of 20 Å diameter, while Anpo et al.[16] measured shifts of 0.156 eV for 38 Å particles. Given that the poorly crystalline precipitate investigated here (sample 2) contains crystalline domains with an apparent particle diameter of <20 Å, then these results would seem to be in agreement. On the other hand Serpone et al.[11] have recently studied in detail the optical absorption edges of anatase sols synthesized through arrested hydrolysis of $TiCl_4$ with particle sizes in the range 21−267 Å and found no evidence for band edge shifts and hence quantum size effects. The optical absorption edges of their anatase sols were dominated by direct transitions in what is an otherwise indirect semiconductor. They also noted the lack of consistency in band edge shifts and particle sizes reported in the literature on titania and issued a warning that the use of the effective mass model[17] in describing quantum size effects in titania is premature and tenuous. The direct transitions measured for the present anatase xerogels of 3.42−3.33 eV are lower than the 4.04 eV reported by Serpone et al.,[11] who also used plots of $(F(R) \times h\nu)^2$ versus $h\nu$ and attributed the optical absorption data to the first allowed direct transition. The disparity between these results and ours is difficult to rationalize given that the range of particle sizes examined here covers the range studied by these investigators. Even the large particle commercial anatase does not give such a high value for the direct transition. What seems apparent, therefore, is that the dominant transition/s manifest in the optical absorption edges appear to depend strongly on the preparation of the titania sol and hence on detailed structural aspects of the titania particles present in the studied sols.

It is useful to compare the E_g values obtained for samples 1 and 2 with that for ETS-10, a titanium silicate containing isolated infinite chains of corner-sharing TiO_6 octahedra. For this material we measured an E_g of 4.00 eV using a method similar to that for the anatase samples. This value of E_g is in agreement with the value calculated by assuming that the linear chains in this compound constitute a quantum wire that can be described by the effective mass approximation.[18] The experimental E_g value for ETS-10 of 4.0 eV is much higher than for samples 1 and 2, and this suggests that the titania precipitate is a condensed system containing more or less extensive domains of connected Ti-containing polyhedra such as in bulk anatase. In a recent study of zeolite-hosted mononuclear Ti-oxide species, Klaas et al.[19] have shown that such species give UV−vis spectra with apparent absorption onsets above about 3.7 eV. These spectra are dominated by O $2p \rightarrow$ Ti $3d$ charge transfer bands at 4.46, 5.59, and 6.08 eV due to mononuclear Ti species having differing coordination numbers and having varying numbers of bonds to the zeolite surface hydroxyls. These bands are to be distinguished from those of quantum sized anatase particles in that their intensity is usually greater by an order of magnitude and increases as the coordination number decreases. It is extremely important to carefully consider such facts when evaluating the present results on anatase particles that range in size from 600 Å to less than 20 Å in diameter. Although we observe in the xerogels what is ostensibly a blue shift in absorption onset with decreasing particle size, which is often interpreted as arising from size quantization, it is important to question what effect an increased contribution from coordina-

tively unsaturated TiO_x surface species (i.e., $x < 6$) or from surface Ti species with dangling bonds $OH-Ti-(OTi)_5$ or $H_2O-Ti-(OTi)_5$ would have on the spectra. For large particles with small surface-to-volume ratios such species would contribute little to absorption edges dominated by direct and indirect band gap excitations, while for small particles, their contribution could in fact be significant, and extremely complex spectra would result that would display an apparent shift of the absorption edge. In fact, it is possible to decompose the UV−visible diffuse reflectance spectra of Figure 3a into a number of components rather successfully. Also, it can be noted in Figure 3a that the spectrum for sample 2, aside from showing an obvious shift to higher energy, has greater intensity and also possesses a strong tailing. To test the hypothesis that an increase in the proportion of essentially mononuclear and coordinatively unsaturated TiO_x species can mimic an absorption edge shift it would be necessary to prove the existence of such species. One technique that is in principle capable of providing such information is XAS.

XANES. The XANES of an X-ray absorption spectrum can be conveniently divided into two regions. The first region, herein called the preedge, is the low-energy region between the absorption threshold and the absorption jump, while the postedge region extends to about 50 eV past the continuum threshold. The preedge region arises from transitions of electrons to bound excited electronic states but this electronic excitation, occurring at the absorbing atom, is strongly modulated by the surrounding atoms in the short to medium range (<100 absorbing atoms) environment. The preedge region therefore contains much potentially useful structural and electronic information but a rigorous theoretical framework does not yet exist to help extract this information. The two most popular approaches to the interpretation of XANES are through multiple scattering and band structure calculations, which are different ways of calculating the same unoccupied density of states. These two different approaches are exemplified in the recent papers of Wu et al.[20] who used a multiple scattering type approach and Parlebas et al.[21] using a configuration-interaction model to simulate the preedge region of the anatase Ti K-edge XANES. Both approaches are able to reproduce at least three (A1, A3, B) of the four preedge features usually observed for anatase and labeled A1−A3 and B. The feature labeled A2 is sometimes observed as a weak shoulder on the low energy side of the A3 peak and requires good energy resolution to be observed. Because the intensity of the preedge transitions are sensitive to the symmetry of the surrounding atoms, being dipole forbidden, they are weak in symmetrical environments and increase in intensity as the environment is distorted. This effect has led to the extensive use of preedge spectra for establishing the coordination of titanium in oxide compounds on a purely empirical basis.

The XANES of titania compounds synthesized by hydrolysis of titanium alkoxides (samples 1−5) are shown in Figure 4 along with the spectrum of a commercial crystalline anatase (sample 7). The preedge spectrum of crystalline anatase (sample 7) which has a somewhat distorted TiO_6 octahedron ($4 \times Ti-O = 1.939$ Å, $2 \times Ti-O = 1.980$ Å) is similar to published spectra. It contains the characteristic triplet structure due to the 1s → 3d core level excitations described above. However, in addition to the three obvious peaks labeled A1, A3, and B, a fourth peak, A2, is indicated on the low-energy side of the central A3 peak. The labeling scheme is in keeping with most recent conventions.[20,21] Because of the small energy separation between the weaker A2 peak and A3, good energy resolution is required

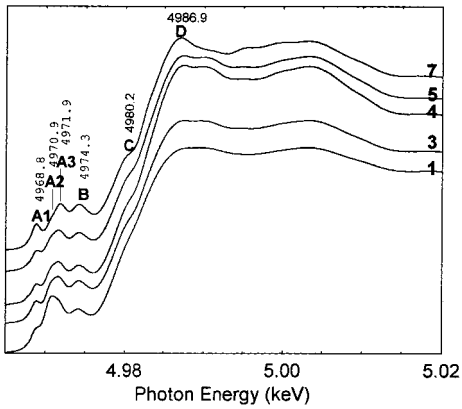

Figure 4. XANES of selected samples in the range 4.96−5.02 keV. Important features are labeled A1−D.

for observation of the former. For instance, A2 is not noted in early studies of anatase preedge structure[22,23] but is in later work.[22] However, in addition to the preedge peaks described so far that have been observed by others, we also note the existence in the XANES of the xerogels weak features to the low-energy side of the A1 transition that have not been previously reported. These are unlikely to be experimental artifacts since they are not observed in the preedge of the commercial sample recorded under identical conditions. Their origin is unknown at this time.

Despite the similarity between the crystallographic and electronic structure of anatase and rutile, the A2 peak does not appear to be present in the XANES of the thermodynamically more stable rutile phase. There is general agreement in recent studies of the anatase Ti K-edge XANES that A3 and B are due to dipole forbidden transitions of the core electron to *b1,e* (3d−4p) and *b2,a1* (3d−4p) hybridized states.[20,21] There is, however, less unanimity regarding the assignment of the A1 and A2 transitions. The A1 peak has been attributed to the core-hole potential and has been shown to have predominantly quadrupole character on the basis of its orientation dependence.[21] In contrast, Wu et al.[20] on the basis of multiple scattering theory, attribute A1 to transitions to 3d−4p hybridized states. There is even less certainty regarding the assignment of the A2 feature. Whereas Wu et al.[20] give A2 a similar origin to the other A series transitions (i.e., 1s → *b2,e* (3d−4p)), Parlebas et al.[21] do not distinguish the A2 and A3 peaks in their theoretical spectra, although they make specific mention of the fact that the experimental preedge of anatase needs four Lorentzian lines for satisfactory decomposition. However, the spectra of Parlebas et al. do reproduce the experimental spectra rather well in terms of both energy and intensity. The fact that the anatase preedge very much depends on medium range structure between 50 and 90 Å from the imbedded Ti atom is emphasized through both of these diverse theoretical approaches.

The postedge region of the Ti K-edge XANES from 4.98 to about 5.02 keV contains a number of poorly resolved and understood intense 3s → *n*p dipole-allowed transitions. In the commercial anatase (sample 7) shown in Figure 4 a number of features can be observed in the postedge region beyond the D transition and these become more poorly resolved as the anatase particle diameter decreases. In the preedge region, quite pronounced differences are also observed as a function of particle size. For sample 7 with the largest particle size, the A1, A3, and B features can be clearly observed while the A2 feature is weak but discernible. As the anatase particle size decreases, the A2 shoulder becomes more pronounced and appears to dominate for the aged precipitate, sample 2. The

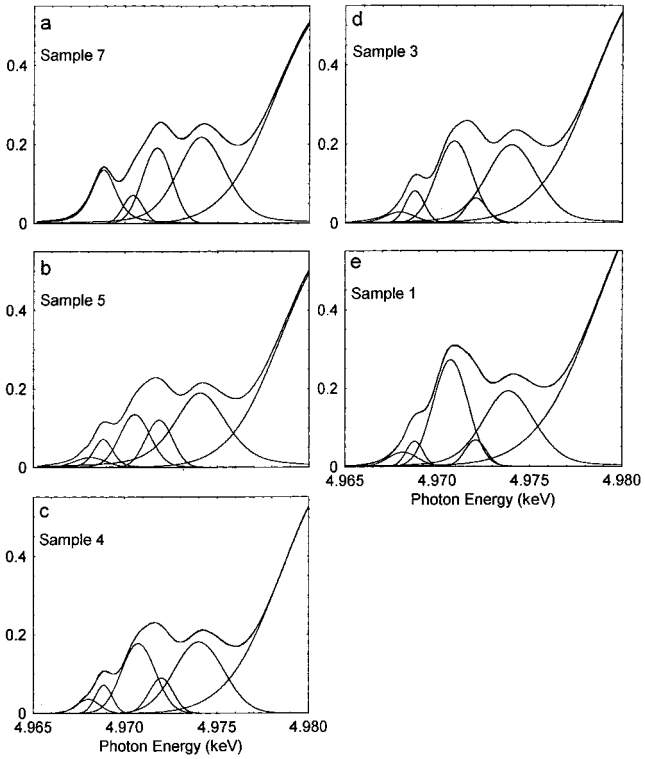

Figure 5. XANES of selected samples in the range 4.965−4.980 keV fitted to pseudo-Voigt line shapes to extract approximate relative intensities of transition.

XANES of the fresh precipitate, sample 1, is not shown but gave an identical preedge to that of sample 2.

In Figure 5 are shown the same series of XANES as in Figure 4 except over a narrower energy range (4.965 to 4.980 keV). Visual inspection of these data over a narrow energy range suggests that for all the samples at least four preedge peaks are present and that the intensities of the A2 and A3 peaks are strongly modulated as crystallite size changes. These data have been decomposed into a number of pseudo-Voigt line shapes in order to extract relative peak areas. The Lorentzian-to-Gaussian ratio has been included as an adjustable parameter in these XANES fits. The use of pseudo-Voigt line profiles is considered justified as the disordered nature of the absorber environment and instrumental effects should impart a Gaussian character to the perfect absorber line shape due to the core-hole, which should be Lorentzian. By fitting these data over a limited energy range up to only the rising edge of the C feature, it is the C peak itself that provides the background for all lower energy features. This approach, applied in a consistent manner to all of the data to be compared, allows useful relative peak area information to be obtained. Employing this approach it is shown that the intensity ratio of the A2 to A3 transitions increases as particle size decreases. The ratio I_{A2}/I_{A3} is plotted in Figure 6a against average particle diameters and highlights the dramatic decrease in the relative contribution made by A2 as the particle diameter increases. If, instead of particle diameter, I_{A2}/I_{A3} is plotted against the surface-to-volume ratio (calculated assuming spherical particles), a linear relationship is suggested. This in turn suggests that the A2 peak may arise predominantly from the surface structure of the anatase particles and/or from Ti species associated with the surface. Recent theoretical treatments of the anatase XANES that have produced good agreement between experimental and theoretical preedge fail to reproduce the A2 feature although its presence is noted in the experimental spectra without explanation.[21] This reinforces

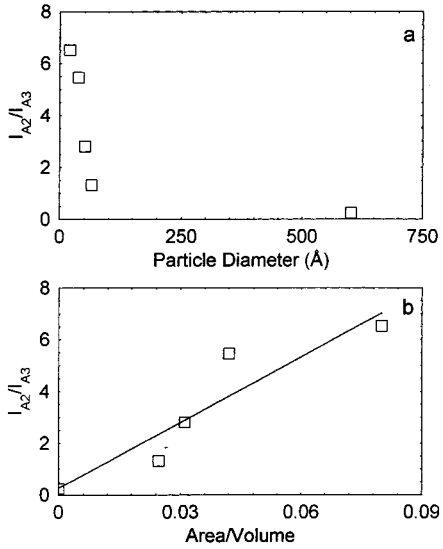

Figure 6. (a) Ratio of the areas of A2 to A3 against average particle diameters and (b) ratio of the areas of A2 to A3 against surface-to-volume ratio.

the suggestion that A2 is not necessarily associated with the bulk anatase density of states but has different origins. If A2 is associated mainly with the poorly crystalline surface regions of the nanocrystals, the exact Ti coordination in these regions must be considered.

Recently, Farges et al.[24,25] showed empirically that the average coordination number of Ti in a range of titanium oxide reference materials and titanium silicate glasses can be extracted reasonably well from plots of preedge intensity versus peak positions. For condensed systems such as anatase and rutile the correlation used the most intense of the preedge peaks, namely A3. Indeed, 4-, 5-, and 6-fold coordinate Ti appears to give preedge peaks at 4969.5, 4970.5, and 4971.5 ± 0.2 eV, respectively. On this basis, the A2 XANES feature, which is observed at 4970.7 ± 0.2 eV in all of the spectra and which predominates in samples 1 and 2, is consistent with five-coordinate Ti. The normalized preedge height of 0.27 is also consistent with this assignment being at the border of that expected for 5- and 6-fold coordination. Therefore the present results suggest that there is a reduction in average coordination number of the titanium as the particle surface makes a larger contribution. Although the effect on the preedge of an increased distortion through a reduction in coordination number is now well established, the effects of progressively distorting a Ti octahedron has not been quantified in such detail. Such a distortion of a Ti octahedron would, however, not be expected to modulate preedge structure to the same degree as distortion created by reducing coordination number. We therefore consider it more likely that the changes observed in preedge structure with crystallite size are due to an increased contribution from five-coordinate Ti species situated on the crystallite surfaces.

EXAFS. The magnitude Fourier transform (FT) EXAFS (uncorrected for phase shift) of a selection of samples of different particle sizes is shown in Figure 7. These FTs show the existence of three shells of back-scattering atoms around the central Ti. As shown from calculation (FEFF 5.05) on a theoretical anatase structure, the first and second shells in these Fourier transforms are from single scattering paths, Ti−O and Ti−Ti, respectively. The third FT peak contains single and multiple scattering contributions from a variety of paths such as Ti−O, Ti−Ti, Ti−Ti−O, Ti−O−Ti−O, etc. The main observation to be made from the data in Figure 7 is that there

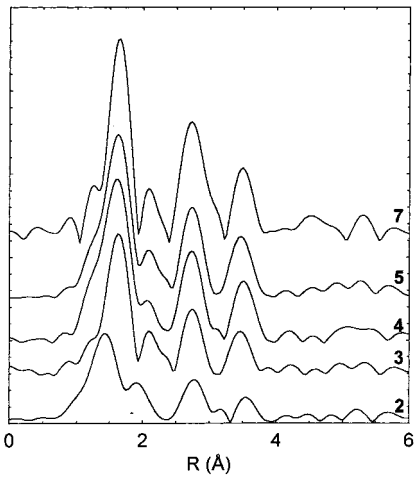

Figure 7. Normalized magnitude FT EXAFS of selected samples.

is a general reduction in amplitude of the FT peaks with decreasing particle size. Also, peaks from higher shells decrease in intensity relative to the first shell peak as particle size decreases. These changes indicate that the nearest (Ti−O) and next nearest neighbor (Ti−Ti) shells experience an increase in mean square relative displacement (MSRD) with decreasing crystallinity and that this affects the latter even more. Similar observations have been made for CdS nanoparticles.[26] Conspicuous in this series of FT EXAFS plots is the lower first neighbor distance observed for sample 2.

Fitting of the EXAFS was undertaken to obtain structural parameters, and to ascertain how these varied as the crystallite size changed. The strategy used to fit the data was to begin with the most crystalline sample (7, the commercial anatase), fix the coordination numbers N, distances R, and Debye−Waller factors σ^2 at the values expected for crystalline anatase, and then float the energy zero E0 and the amplitude reduction factor S_o^2. The EXAFS Debye−Waller factors were obtained from the corresponding X-ray diffraction values[27] using the equation of Teo:[28]

$$\sigma_{AB}{}^2 = \langle(\mathbf{r}_{AB}\cdot U_A)^2\rangle + \langle(\mathbf{r}_{AB}\cdot U_B)^2\rangle - 2\langle(\mathbf{r}_{AB}\cdot U_B)(\mathbf{r}_{AB}\cdot U_A)\rangle$$

Here $\mathbf{r}_{AB}$ is the unit vector along A−B and U_A and U_B are the instantaneous coordinates of A and B obtained from the XRD. The third term is a correlation term, and assuming for the present purposes that the motions of A and B are uncorrelated, it is neglected. Using this equation and the results of Howard et al.[27] we calculate that $\sigma_{TiO}^2 = 0.0010$. The structural parameters obtained from the commercial anatase fit were then used as initial input into fitting of the nanocrystalline samples. The coordination numbers and Debye−Waller factors in disordered systems are usually strongly correlated; thus the values obtained by least-squares fitting are a measure of disorder rather than precisely determined parameters. An additional complication in disordered systems is that the pair distribution function may not be symmetrical; anharmonicity in the pair potential can cause an underestimation of both distance and coordination numbers.[29,30] For the data obtained here, however, attempts to include a third cumulant term, which contributes to the phase in an anharmonic fit, resulted in convergence of this term to zero for all samples except number 1. For sample 1 the goodness of fit achieved with an anharmonic term included was not significantly better than that achieved without; accordingly, the harmonic approximation was preferred for this sample also.

As noted above, the third peak in the Fourier transforms contains many contributions from both single and multiple scattering paths. For the disordered systems studied here, this peak was fitted with a single set of N, r, and σ^2 values that have no structural significance.

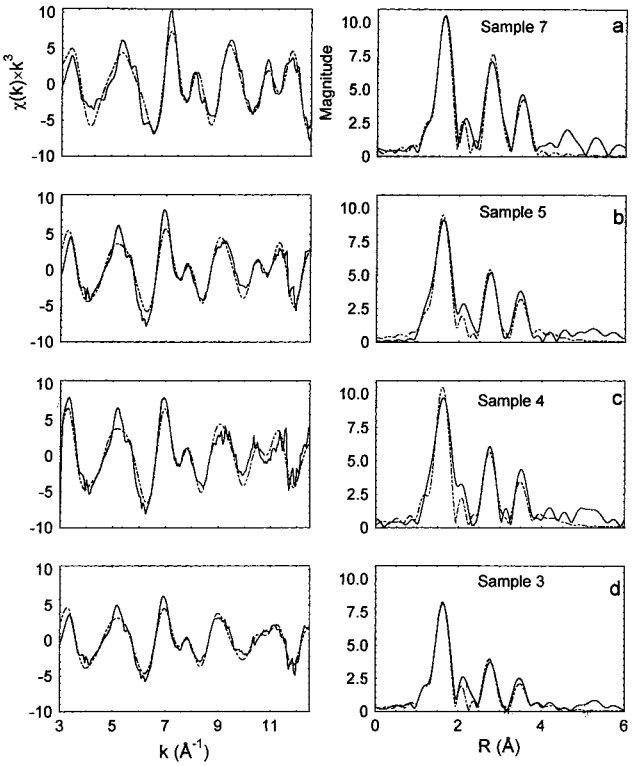

Figure 8. Fitted k^3-weighted Ti k-edge EXAFS (left) and corresponding fitted magnitude FT spectra (right) of (a) commercial anatase from Aldrich, sample 7; (b) xerogel dried in air at 300 °C, sample 6; (c) dried xerogel calcined at 200 °C, sample 5; and (d) dried xerogel calcined at 30 °C, sample 3.

TABLE 2: EXAFS Fit Results for Titania Powder Samples of Varying Crystallite Size

sample	shell	N	R (Å)	σ^2 (Å^2)
T[a]	O	4	1.9339	
	O	2	1.9795	
	Ti	4	3.0394	
	Ti	4	3.7845	
	O	8	3.8570	
1	O	2.0	1.85	0.001
	O	1.9	2.01	0.003
	Ti	2.1	3.09	0.014
3	O	4.9	1.95	0.002
	Ti	2.8	3.07	0.004
	Ti, O[b]	9.3	3.87	0.003
4	O	5.9	1.94	0.002
	Ti	5.1	3.05	0.006
	Ti, O[b]	16.9	3.88	0.005
5	O	6.4	1.94	0.003
	Ti	3.5	3.05	0.003
	Ti, O[b]	10.3	3.88	0.003
6	O	5.3	1.94	0.005
	Ti	1.9	3.05	0.002
	Ti, O[b]	5.0	3.88	0.001
7	O	6.0	1.94	0.001
	Ti	4.0	3.05	0.002
	Ti, O[b]	16.6	3.88	0.004

[a] From crystallographic data. [b] Single and multiple scattering paths containing Ti and O contribute to this shell.

Figure 8 shows the observed and best-fit calculated EXAFS and magnitude Fourier transforms for samples 3−7. The best fit parameters for these samples are listed in Table 2. All could be fitted with single Ti−O first shells and coordination numbers

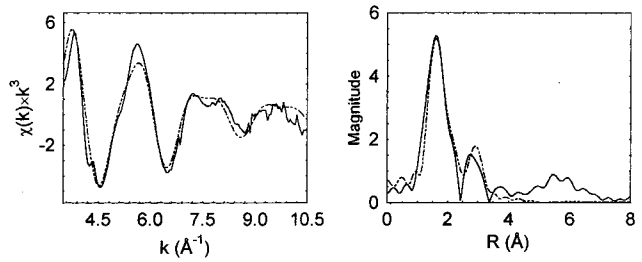

Figure 9. Fitted k^3-weighted Ti *k*-edge EXAFS spectra (left) and corresponding fitted magnitude FT spectra (right) of amorphous precipitate (sample 1).

of close to six; the Debye−Waller factors for this first shell show some increase over that for crystalline anatase. The Ti−O distances are very close to the average value for anatase (1.947 Å). The Ti−Ti second shell coordination numbers show more variation from that of crystalline anatase, but this is probably due to the correlation between N and σ^2. The Ti−Ti distances are close to those of the crystalline anatase.

Figure 9 shows corresponding data for sample 1. The EXAFS for this sample could not be fitted with the same single Ti−O shell as the others, but required two shells at 1.85 and 2.01 Å respectively. An average Ti−O bond length of 1.85 Å is between that observed in compounds containing five-coordinate Ti (as $O_4Ti{=}O$) such as $K_2Ti_2O_5$[31] and fresnoite[32] with average Ti−O bond lengths of 1.89 and 1.91 Å, respectively, and four-coordinate Ti such as in $Ni_{2.4}Ti_{0.7}Si_{0.05}O_4$ spinel[33] and β-Ba_2TiO_4[34] with average Ti−O bond lengths of 1.823 and 1.81 Å. A Ti−O bond length of around 1.85 Å was found by EXAFS[35] for an amorphous sol−gel derived precipitate, although no evidence for a reduced coordination number was observed in the XANES region. Contracted Ti−O bond lengths have also been reported very recently[36] for a series of anatase gels containing crystallites less than 50 Å in size. The fitting results for sample 1 are thus consistent with these other reports of short Ti−O bonds in very small titania crystallites.

The total first shell Ti−O coordination number for sample 1 is lower than that for crystalline anatase, although the uncertainties in Debye−Waller factors mean that the value obtained from least-squares fitting of the data is not reliable. However, this value together with the contracted Ti−O bond length and the XANES evidence discussed above makes it clear that this sample contains titanium in lower coordination. The reduced Ti−Ti second shell coordination is an indication of increased disorder in this sample (note the increased Debye−Waller factor).

In studies of anatase surface sensitization it is often postulated that incompletely coordinated Ti surface atoms act as electron-trapping centers. However, there appears to be little experimental evidence that this is so.[37,38] Clearly, before such hypothetical sites can be implicated in interfacial electron-transfer processes, their existence needs to be proved. There is ample evidence for the existence of a variety of intrinsic defects on the surface of anatase single crystals. Oxygen vacancies at bridging and in plane positions represent one type of surface defect present on annealed titania surfaces and evidence for their existence has come from assorted surface science techniques including STM.[39] Oxygen vacancies result in coordinatively unsaturated Ti atoms or Lewis acid sites. Under ambient conditions these vacant coordination positions might be expected to be occupied by water molecules that can then dissociate to give OH groups. Indirect infrared spectroscopic evidence for the irreversible formation of five-coordinate Ti on microcrystalline anatase after mild heating to 150 °C was provided some time ago.[40,41] Recent theoretical studies of the anatase surface suggests that there are two types of five-coordinate Ti sites on anatase surfaces and that only one of these coordinates water.[42] We believe that the present study provides direct empirical evidence for the existence of coordinatively unsaturated Ti atoms in anatase crystallites even under hydrated conditions. One possible reason such sites can can exist even under ambient conditions may be that access to the coordination sites is sterically hindered.

Conclusions

The apparent band gaps of nanocrystalline anatase samples do not vary in a simple way with particle size. The caution expressed by Serpone et al.[11] over interpretation of apparent band gap shifts is reiterated here. The presence of defect and surface states in the band gap has a strong influence on the optical absorption spectrum, and is strongly dependent on sample preparation conditions. On the other hand, the intensity of the A2 peak in the Ti K-edge XANES does appear to vary systematically with particle size. The correlation between the A2:A3 intensity and the surface-to-volume ratio suggests that the A2 peak is associated with the surface of the anatase particles. Furthermore, the position of this peak indicates a reduced coordination number for titanium in the surface region.

Ti K-edge EXAFS measurements confirm the presence of contracted Ti−O bonds consistent with reduced coordination number in the smallest anatase particles studied. The EXAFS of larger particles is dominated by contributions from the bulk phase, and surface effects cannot be clearly seen (although the disorder apparent in Debye−Waller factors and second shell coordination numbers may be related to surface-to-volume ratios).

Work is in progress to quantify further the effects seen here, in particular, to obtain accurate Debye−Waller factors by measuring temperature dependent EXAFS from a series of well-characterized titania sols, so that more reliable coordination numbers can be obtained. The presence of disordered and coordinatively unsaturated titanium at the surface of nanocrystalline anatase particles may have important implications for the photoreactivity of these systems.

Acknowledgment. This work was supported by the Australian Research Council. Access to the Photon Factory was provided by the Australian Synchrotron Research Program, which has been funded by the Commonwealth of Australia via the Major National Research Facilities Program. Access to SSRL was funded by the Access to Major Research Facilities Program of DIST. We acknowledge also provision of beam time on BL4-1 at SSRL and assistance of SSRL staff. SSRL is funded through the U.S. Department of Energy and the National Institutes of Health.

References and Notes

(1) Sclafani, A.; Herrmann, J. M. *J. Phys. Chem.* **1996**, *100*, 13655.
(2) O'Regan, B.; Moser, J.; Anderson, M.; Grätzel, M. *J. Phys. Chem.* **1990**, *94*, 8720.
(3) O'Regan, B.; Grätzel, M. *Nature* **1991**, *353*, 737. Duonghong, D.; Ramsden, J.; Grätzel, M. *J. Am. Chem. Soc.***1982**, *104*, 2977. O'Regan, B.; Grätzel, M.; Fitzmaurice, D. *J. Phys. Chem.* **1991**, *95*, 10525. Rothenberger, G.; Fitzmaurice, D.; Grätzel, M. *J. Phys. Chem.* **1992**, *96*, 5983. Hagfeldt, A. Bjõrkstén, U.; Grätzel, M. *J. Phys. Chem.* **1996**, *100*, 8045. Bahnemann, D.; Henglein, A.; Lilie, J.; Spanhel, L. *J. Phys. Chem.* **1984**, *88*, 709.
(4) Zhu, Z.; Tsung, L.; Tomkiewicz, M. *J. Phys. Chem.* **1995**, *99*, 15945.
(5) Zhi, Z.; Lin, M.; Dagan, G.; Tomkiewicz, M. *J. Phys. Chem.* **1995**, *99*, 15950.
(6) Skinner, D. E.; Colombo, D. P.; Cavaleri, J. J.; Bowman, R. M. *J. Phys. Chem.* **1995**, *99*, 7853. Zhang, J. Z. *Acc. Chem. Res.* **1997**, *30*, 423.

(7) Ressler, T. *J. Phys. IV* **1997**, *7*, 269.
(8) Ellis, P. A.; Freeman, H. C. *J. Synchrotron Rad.* **1995**, *2*, 190.
(9) Stern, E. A.; Newville, M.; Ravel, B.; Yacoby, Y.; Haskel, D. *Physica B* **1995**, *208 & 209*, 117.
(10) Klug, H. P.; Alexander, L. E. *X-ray Diffraction Procedures for Polycrystalline and Amorphous Materials*; Wiley: New York, 1974.
(11) Serpone, N.; Lawless, D.; Khairutdinov, R. *J. Phys. Chem*. **1995**, *99*, 16646.
(12) Sanchez, E.; Lopez, T. *Mater. Lett.* **1995**, *25*, 271.
(13) Lassaletta, G.; Fernandez, A.; Espinos, J. P.; Gonzalez-Elipe, A. R. *J. Phys. Chem*. **1995**, *99*, 1484.
(14) Frova, A.; Boddy, P. J.; Chen, Y. S. *Phys. Rev.* **1967**, *157*, 700.
(15) Bahnemann, D. W. *Isr. J. Chem*. **1993**, *33*, 115.
(16) Anpo, M.; Shima, T.; Kodama, S.; Kubokawa, Y. *J. Phys. Chem*. **1987**, *91*, 4305.
(17) Brus, L. *J. Phys. Chem.* **1986**, *90*, 2555. Brus, L. *J. Chem. Phys.* **1984**, *80*, 4403. Brus, L. *IEEE J. Quantum Electron.* **1986**, *QE22*, 1909.
(18) Borello, E.; Lamberti, C.; Bordiga, S.; Zecchina, A.; Arean, C. O. *Appl. Phys. Lett*. **1997**, *71*, 2319.
(19) Klaas, J.; Schulz-Ekloff, G.; Jaeger, N. I. *J. Phys. Chem*. **1992**, *96*, 1305.
(20) Wu, Z. Y.; Ouvrard, G.; Gressier, P.; Natoli, C. R. *Phys. Rev.* **1997**, *B55*, 10382.
(21) Parlebas, J. C.; Khan, M. A.; Uozumi, T.; Okada, K.; Kotani, A. *J. Electron Spectrosc. Relat. Phenom*. **1995**, *71*, 117.
(22) Grunes, L. A. *Phys. Rev.* **1983**, *B27*, 2111.
(23) Brydson, R.; Sauer, H.; Engel W.; Thomas, J. M.; Zeitler, E.; Kosugi, N.; Kuroda, H. *J. Phys.: Condensed Matter* **1989**, *1*, 797.
(24) Farges, F. *Am. Mineral.* **1997**, *92*, 44.
(25) Farges, F.; Brown, G. E., Jr.; Rehr, J. J. *Geochim. Cosmochim. Acta* **1996**, *60*, 3023.
(26) Rockenberger, J.; Tröger, L.; Kornowski, A.; Vossmeyer, T.; Eychmüller, A.; Feldhaus, J.; Weller, H. *J. Phys. Chem*. **1997**, *101*, 2691.
(27) Howard, C. J.; Sabine, T. M.; Dickson, F. *Acta Crystallogr*. **1991**, *B47*, 462.
(28) Teo, B. K. *EXAFS: Basic Principles and Data Analysis*; Springer-Verlag; New York, 1986.
(29) Crozier, E. D.; Rehr, J. J.; Ingalls, R. Amorphous and Liquid Systems. In *X-ray Absorption;* Principles, Applications, Techniques of EXAFS, SEXAFS and XANES; Koningsberger, D. C., Prins, R. Eds.; Chem. Anal. **92:** 373−442.
(30) Farges, F.; Brown, G. E., Navrotsky, A.; Gan, H.; Rehr, J. R. *Geochim. Cosmochim. Acta* **1996**, *60*, 3055.
(31) Andersson, S.; Wadsley, A. D. *Acta Chem. Scand*. **1974**, *15*, 663.
(32) Markgraf, S. A.; Halliyal, A.; Bhalla, A. S.; Prewitt, C. T. *Ferroelectrics* **1985**, 62, 17.
(33) Larger, G. A.; Armbruster, T.; Ross, F. K.; Rotella, F. J.; Jorgensen, J. D. *J. Appl. Crystallogr*. **1981**, *14*, 261.
(34) Wu, B. K. K.; Brown, I. D. *Acta Crystallogr*. **1973**, *B29*, 2009.
(35) Manzini, I.; Antonioli, G.; Lottici, P. P.; Gnappi, G.; Montenero, A. *J. Non-Cryst. Solids* **1995**, *192 & 193*, 519.
(36) Chen, L. X.; Rajh, T.; Wang, Z.; Thurnauer, M. C. *J. Phys. Chem*. **1997**, *101*, 10688.
(37) Redmond, A.; Fitzmaurice, D.; Grätzel, M. *J. Phys. Chem.* **1993**, *97*, 6951.
(38) Boschloo, G. K.; Goossens, A. *J. Phys. Chem.* **1996**, *100*, 19489.
(39) Fischer, S.; Munz, A. W.; Schierbaum, K.-D. Gopel W. *Surf. Sci*. **1995**, *337*, 17.
(40) Primet, M.; Pichat, P.; Mathieu, M.-V. *J. Phys. Chem.* **1971**, *75*, 1216.
(41) Primet, M.; Pichat, P.; Mathieu, M.-V. *J. Phys. Chem.* **1971**, *75*, 1221.
(42) Lindan, P. J. D.; Muscat, J.; Bates, S.; Harrison, N. M.; Gillan, M. *Faraday Discuss.* **1997**, *106*, 135−154.